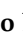











Article

A Novel Approach to β -Decay: PANDORA, a New Experimental Setup for Future In-Plasma Measurements

David Mascali ^{1,*}, Domenico Santonocito ¹, Simone Amaducci ¹, Lucio Andò ¹, Vincenzo Antonuccio ², Sándor Biri ³, Alfio Bonanno ^{1,2}, Vincenza Piera Bonanno ¹, Stefan Briefi ⁴, Maurizio Busso ^{5,6}, Luigi Celona ¹, Luigi Cosentino ¹, Sergio Cristallo ^{6,7}, Marco Cuffiani ⁸, Costantino De Angelis ^{9,10}, Giacomo De Angelis ^{11,12}, Davide De Salvador ^{11,13}, Loreto Di Donato ^{1,14}, Jean-Eric Ducret ¹⁵, Aref Eshkevar Vakili ¹, Ursel Fantz ⁴, Alessio Galatà ¹¹, Carmelo Sebastiano Gallo ^{11,16}, Santo Gammino ¹, Tommaso Isernia ^{1,17}, Hannu Koivisto ¹², Karl-Ludwig Kratz ¹⁸, Risto Kronholm ¹², Marco La Cognata ¹, Silvia Leoni ^{10,19}, Andrea Locatelli ^{9,10}, Mario Maggiore ¹¹, Fabio Maimone ²⁰, Luciana Malferrari ⁸, Giorgio Mancini ²¹, Laurent Maunoury ¹⁵, Giorgio Sebastiano Mauro ¹, Maria Mazzaglia ¹, Alberto Mengoni ^{8,22}, Andrea Miraglia ¹, Bharat Mishra ^{1,23}, Mario Musumeci ¹, Daniel Ricardo Napoli ¹¹, Eugenia Naselli ¹, Fabrizio Odorici ⁸, Libero Palladino ²⁴, Giuseppe Palmisano ¹⁴, Santi Pavone ^{1,14}, Salvatore Pennisi ¹⁴, Albino Perego ²⁵, Angelo Pidotella ¹, Richard Rácz ³, Riccardo Reitano ^{1,23}, Danilo Rifuggiato ^{1,11}, Matteo Rinaldi ^{5,6}, Antonio Domenico Russo ¹, Filippo Russo ²⁶, Gaetano Schillaci ¹, Stefano Selleri ^{11,27}, Stefano Simonucci ^{6,21}, Gino Sorbello ^{1,14}, Roberta Sparta ¹, Simone Taioli ^{28,29,30}, Klaus Tinschert ²⁰, Giuseppe Torrisi ¹, Antonio Trifirò ³¹, Sedina Tsikata ³², Aurora Tumino ^{1,33}, Diego Vescovi ³⁴ and Luca Vincetti ^{10,35}



Citation: Mascali, D.; Santonocito, D.; Amaducci, S.; Andò, L.; Antonuccio, V.; Biri, S.; Bonanno, A.; Bonanno, V.P.; Briefi, S.; Busso, M.; et al. A Novel Approach to β -Decay: PANDORA, a New Experimental Setup for Future In-Plasma Measurements. *Universe* **2022**, *8*, 80. <https://doi.org/10.3390/universe8020080>

Academic Editor: Alexander S. Barabash

Received: 5 December 2021

Accepted: 17 January 2022

Published: 27 January 2022

Publisher's Note: MDPI stays neutral with regard to jurisdictional claims in published maps and institutional affiliations.



Copyright: © 2022 by the authors. Licensee MDPI, Basel, Switzerland. This article is an open access article distributed under the terms and conditions of the Creative Commons Attribution (CC BY) license (<https://creativecommons.org/licenses/by/4.0/>).

- ¹ National Institute for Nuclear Physics (INFN)-Laboratori Nazionali Del Sud, 95125 Catania, Italy; santonocito@lns.infn.it (D.S.); amaducci@lns.infn.it (S.A.); lucioando@gmail.com (L.A.); alfio.bonanno@inaf.it (A.B.); bonanno@lns.infn.it (V.P.B.); celona@lns.infn.it (L.C.); cosentino@lns.infn.it (L.C.); loreto.didonato@dieei.unict.it (L.D.D.); aref.vakili@optoi.com (A.E.V.); gammino@lns.infn.it (S.G.); tommaso.isernia@unirc.it (T.I.); lacognata@lns.infn.it (M.L.C.); mauro@lns.infn.it (G.S.M.); mazzaglia@lns.infn.it (M.M.); miraglia@lns.infn.it (A.M.); mishra@lns.infn.it (B.M.); musumeci@lns.infn.it (M.M.); eugenia.naselli@lns.infn.it (E.N.); santi.pavone@unict.it (S.P.); pidatella@lns.infn.it (A.P.); riccardo.reitano@ct.infn.it (R.R.); rifuggiato@lns.infn.it (D.R.); antonio.russo@lns.infn.it (A.D.R.); schillaci@lns.infn.it (G.S.); gino.sorbello@unict.it (G.S.); rsparta@lns.infn.it (R.S.); peppetorrisi@lns.infn.it (G.T.); tumino@lns.infn.it (A.T.)
- ² National Institute for Astrophysics (INAF)-Astrophysical Observatory of Catania, 95123 Catania, Italy; vincenzo.antonuccio@inaf.it
- ³ Institute for Nuclear Research (ATOMKI), 4026 Debrecen, Hungary; biri@atomki.hu (S.B.); rracz@atomki.hu (R.R.)
- ⁴ Max Planck Institute-Institute of Plasma Physics, 85748 Garching, Germany; stefan.briefi@physik.uni-augsburg.de (S.B.); ursel.fantz@ipp.mpg.de (U.F.)
- ⁵ Department of Physics and Geology, University of Perugia, 06123 Perugia, Italy; maurizio.busso@pg.infn.it (M.B.); matteo.rinaldi@pg.infn.it (M.R.)
- ⁶ National Institute for Nuclear Physics (INFN)-Sez. di Perugia, 06123 Perugia, Italy; cristallo@oa-teramo.inaf.it (S.C.); stefano.simonucci@unicam.it (S.S.)
- ⁷ National Institute for Astrophysics (INAF), Astrophysical Observatory of Abruzzo, 64100 Teramo, Italy
- ⁸ National Institute for Nuclear Physics (INFN)-Sez. di Bologna, 40127 Bologna, Italy; marco.cuffiani@bo.infn.it (M.C.); luciana.malferrari@bo.infn.it (L.M.); alberto.mengoni@enea.it (A.M.); fabrizio.odorici@bo.infn.it (F.O.)
- ⁹ Department of Information Engineering, Università degli Studi di Brescia, Via Branze 38, 25123 Brescia, Italy; costantino.deangelis@unibs.it (C.D.A.); andrea.locatelli@unibs.it (A.L.)
- ¹⁰ National Institute for Nuclear Physics (INFN)-Sez. di Milano, 20133 Milano, Italy; silvia.leoni@mi.infn.it (S.L.); luca.vincetti@unimore.it (L.V.)
- ¹¹ National Institute for Nuclear Physics (INFN)-Laboratori Nazionali di Legnaro, 35020 Legnaro, Italy; giacomo.deangelis@lnl.infn.it (G.D.A.); davide.desalvador@unipd.it (D.D.S.); alessio.galatà@lnl.infn.it (A.G.); carmelo.gallo@lnl.infn.it (C.S.G.); mario.maggiore@lnl.infn.it (M.M.); daniel.r.napoli@lnl.infn.it (D.R.N.); stefano.selleri@unipr.it (S.S.)
- ¹² Department of Physics, University of Jyväskylä, P.O. Box 35, 40014 Jyväskylä, Finland; hannu.a.koivisto@jyu.fi (H.K.); risto.j.kronholm@jyu.fi (R.K.)
- ¹³ Department of Physics, University of Padova, 35131 Padova, Italy
- ¹⁴ Department of Electrical, Electronics and Computer Engineering, University of Catania, 95126 Catania, Italy; giuseppe.palmisano@unict.it (G.P.); salvatore.pennisi@unict.it (S.P.)

- ¹⁵ GANIL, Boulevard Henri Becquerel, 14076 Caen, France; jean-eric.ducuret@ganil.fr (J.-E.D.); laurent.maunoury@ganil.fr (L.M.)
- ¹⁶ Department of Physics and Earth Science, University of Ferrara, 44122 Ferrara, Italy
- ¹⁷ Dipartimento di Ingegneria dell'Informazione, delle Infrastrutture e dell'Energia Sostenibile, Università Mediterranea di Reggio Calabria, 89124 Reggio Calabria, Italy
- ¹⁸ Institute for Nuclear Chemistry, Johannes Gutenberg University Mainz, 55122 Mainz, Germany; klk@uni-mainz.de
- ¹⁹ Department of Physics, University of Milano, 20133 Milano, Italy
- ²⁰ GSI Helmholtzzentrum für Schwerionenforschung, 64291 Darmstadt, Germany; f.maimone@gsi.de (F.M.); k.tinschert@gsi.de (K.T.)
- ²¹ Department of Physics, University of Camerino, 62032 Camerino, Italy; giorgio.mancini@unicam.it
- ²² Italian National Agency for New Technologies, Energy and Sustainable Economic Development (ENEA), 40129 Bologna, Italy
- ²³ Department of Physics and Astronomy, University of Catania, 95125 Catania, Italy
- ²⁴ National Institute for Nuclear Physics (INFN)-Sez. dell'Aquila, 67100 L'Aquila, Italy; libero.palladino@aquila.infn.it
- ²⁵ Department of Physics, University of Trento, 38123 Povo, Italy; albino.perego@unitn.it
- ²⁶ National Center for Oncological Hadrontherapy CNAO, 27100 Pavia, Italy; filipporusso90@outlook.com
- ²⁷ Department of Engineering and Architecture, University of Parma, 43124 Parma, Italy
- ²⁸ Trento Institute for Fundamental Physics and Applications, TIFPA-INFN, 38123 Trento, Italy; taioli@ectstar.eu
- ²⁹ European Centre for Theoretical Studies in Nuclear Physics and Related Areas, Fondazione Bruno Kessler, 38123 Trento, Italy
- ³⁰ World-Class Research Center for Advanced Digital Technologies, Peter the Great St. Petersburg Polytechnic University, 195251 St. Petersburg, Russia
- ³¹ Department MIFT, University of Messina, 98122 Messina, Italy; antonio.trifiro@unime.it
- ³² ICARE, CNRS (UPR 3021), 1C ave. de la Recherche Scientifique, 45071 Orléans, France; sedina.tsikata@cnrs-orleans.fr
- ³³ Department of Engineering and Architecture, University of Enna "Kore", 94100 Enna, Italy
- ³⁴ Department of Physics, Goethe University Frankfurt, Max-von-Laue-Strasse 1, 60438 Frankfurt am Main, Germany; vescovi@iap.uni-frankfurt.de
- ³⁵ Department of Engineering "Enzo Ferrari", University of Modena and Reggio Emilia, 41125 Modena, Italy
- * Correspondence: davidmascali@lns.infn.it; Tel.: +39-095-542-587

Abstract: Theoretical predictions as well as experiments performed at storage rings have shown that the lifetimes of β -radionuclides can change significantly as a function of the ionization state. In this paper we describe an innovative approach, based on the use of a compact plasma trap to emulate selected stellar-like conditions. It has been proposed within the PANDORA project (Plasmas for Astrophysics, Nuclear Decay Observation and Radiation for Archaeometry) with the aim to measure, for the first time in plasma, nuclear β -decay rates of radionuclides involved in nuclear-astrophysics processes. To achieve this task, a compact magnetic plasma trap has been designed to reach the needed plasma densities, temperatures, and charge-states distributions. A multi-diagnostic setup will monitor, on-line, the plasma parameters, which will be correlated with the decay rate of the radionuclides. The latter will be measured through the detection of the γ -rays emitted by the excited daughter nuclei following the β -decay. An array of 14 HPGe detectors placed around the trap will be used to detect the emitted γ -rays. For the first experimental campaign three isotopes, ^{176}Lu , ^{134}Cs , and ^{94}Nb , were selected as possible physics cases. The newly designed plasma trap will also represent a tool of choice to measure the plasma opacities in a broad spectrum of plasma conditions, experimentally poorly known but that have a great impact on the energy transport and spectroscopic observations of many astrophysical objects. Status and perspectives of the project will be highlighted in the paper.

Keywords: beta decay; nucleosynthesis; plasma trap; plasma diagnostics

1. Introduction

In the last decades, many experimental and theoretical efforts have been dedicated at investigating various possible scenarios that can influence nuclear decay rates. It has been

predicted that sizeable variations in the decay properties can be observed in highly ionized nuclides. This would have a strong impact on stellar nucleosynthesis processes, which take place in a hot, dense environment affecting the degree of ionization of the atoms involved in the stellar nucleosynthesis processes. However, our present knowledge of the effects of the external environment on the nuclear β -decay rates is rather limited. Early attempts to measure the dependence of the beta decay rates on the temperature, the pressure, or the magnetic field were performed in the 1920s but the results showed variations lower than about 0.05% (see, e.g., [1]). A revival of interest in the field took place near the end of the 1960s with the discovery of a chemically induced change of about 3.5% in the half-life of ^7Be (see, e.g., [1,2]). An important breakthrough in the field was achieved thanks to the use of Storage Rings, due to the possibility of preserving for extended periods of time (up to several hours) highly ionized ions and to map their decay. This opportunity made accessible the so-called “bound-state β -decay” [3]. In some neutral atoms or ions with only a few holes in the atomic levels, the β -decay mechanism is hindered or even blocked because the emitted electron is unable to access a bound final state. Therefore, it needs to be emitted with high kinetic energy, which is sometimes not possible in terms of energy conservation. However, in highly ionized ions the decay becomes possible or, somehow, energetically favored. Experimental results obtained in a storage ring showed, for example, that fully stripped $^{187}\text{Re}^{75+}$ ions decayed by 9 orders of magnitude faster than neutral ^{187}Re atoms, which have a half-life of 42 Gyr [4], and that bare $^{163}\text{Dy}^{66+}$ nuclei, being stable as neutral atoms, become radioactive, with a half-life of 47 days, thus allowing the occurrence of a branching reaction in the s-process path [5]. However, such an approach, being based on the investigations of a single charge state at a time while clearly showing the role played by the high ionization state of an atom in the β -decay process, is not able to reproduce stellar-like conditions where, due to the high temperature of the plasma, a Charge State Distribution (CSD) of the ions is established in Local Thermodynamic Equilibrium (LTE) condition.

In order to elucidate the possible effects connected to the dependence of the beta decay constant on the characteristics of the CSD, a totally new approach was conceived by the PANDORA (Plasmas for Astrophysics Nuclear Decays Observation and Radiation for Archaeometry) project [6,7], to be realized at the Laboratori Nazionali del Sud, Istituto Nazionale di Fisica Nucleare (INFN-LNS). It is based on the use of an innovative plasma trap to measure, for the first time, nuclear β -decay rates in a plasma emulating some stellar-like conditions in terms of CSD.

This paper describes the theoretical background, the experimental approach, and the technical solutions foreseen to achieve this goal. At the same time, complementary information about plasma emissivity and opacity in the range of plasma temperature $kT = 1\text{--}10$ eV and density up to 10^{13} cm^{-3} will be extracted, which could be of crucial interest for benchmarking astrophysical observations from kilonovae [8] through laboratory measurements.

2. Impact in Astrophysical Scenarios

There is great interest in Nuclear Astrophysics for any attempt to gain improved knowledge of weak interactions in physical conditions close to those of nucleosynthesis environments (stars, the Big Bang, and cosmic rays). In fact, while in the last decades our knowledge of the reaction cross sections involved in these processes improved significantly, this was not the case for the weak interaction that presently represents the most important bottleneck in nucleosynthesis calculations. In the s-process (i.e., the slow neutron capture process), as an example, the relative abundances of elements and isotopes produced depend on the interplay between neutron densities (neutron fluxes coming from reactions producing neutrons), neutron capture cross sections, and decay rates. The s-process is a crucial mechanism in the synthesis of about 50% of the nuclei heavier than iron [9]. A significant fraction of neutron capture reactions occurs on unstable nuclei close to the valley of β -stability. However, as highlighted in Section 1, even stable nuclides in terrestrial laboratories may become unstable when ionized. This introduces enormous uncertainties

in the knowledge of the lifetimes of these isotopes, which are exposed to neutron captures over a wide range of time durations, from less than 20 years (in the thermal instabilities of shell He-burning in low mass stars) up to thousands of years in core He-burning conditions of massive stars. The ionization conditions can also open the bound-state β -decay channel in which the produced electron is not emitted but captured in a bound atomic energy state [10]. Very little is known on the effectiveness of such a process in the nucleosynthesis chains, except that for very few nuclei where, as mentioned, the storage ring measurements showed changes in half-lives up to several orders of magnitude [4,5,10]. The lack of this information has also hampered the possibility of using long-lived radionuclides as cosmological chronometers, since uncertainties in their lifetime, associated to their astration in the stars, do not allow being confident in estimating the age of a given astrophysical object by just looking at the relative abundances of certain isotopes (i.e., measuring the “parent–daughter” abundances ratio).

A new approach described in detail in the next paragraphs, based on the use of a plasma trap to emulate some specific stellar-like conditions, will allow us to investigate the β -decay properties of selected radioactive isotopes. The same setup will also provide suitable experimental conditions to study plasma opacity, which quantifies how transparent or opaque the plasma is to radiation. While this last issue will not represent the main item of research, the experimental measurements of this quantity can be a valuable benchmark for supporting more precise estimates of elemental abundances linked to r-process nucleosynthesis derived from direct astrophysical observations of phenomena like kilonovae [8,11]. More in general, also due to the wide set of available diagnostics, PANDORA will be a unique setup for non-LTE plasma atomic physics’ models.

3. Experimental Method

The proposed experimental method consists of magnetically confining a hot plasma, kept in dynamic equilibrium, containing a known concentration of the β -decaying atoms, and then measuring the decay rate vs. time and as a function of the average ionization state of radioactive ions confined in the trap [6]. The decaying nuclei will be identified by measuring the energy of the γ -rays emitted by the daughter nuclei.

The different steps of the method are described below:

- A buffer plasma is created using He, O, or Ar gas at densities of 10^{12} – 10^{13} atoms/cm³.
- The isotope is then directly injected (if gaseous) or vaporized by appropriate ovens in the chamber to be turned into a plasma state.
- Relative abundances of buffer vs. isotope densities range from 100:1 (for isotopes in metallic state) to 3:1 (for gaseous elements).
- The plasma is maintained in a dynamic equilibrium by equalizing input fluxes of the particles to the losses from the magnetic confinement. This can be achieved when the plasma operates in magneto-hydrodynamic equilibrium under proper tuning conditions of the magnetic field profile, background pressure, and radiofrequency (RF) power; an accuracy of about 7% (estimated using the fastest response diagnostics, i.e., soft-X ray spectroscopy, see Table 2) can be achieved in terms of the maximal fluctuation of the main plasma parameters, which are deemed to be sufficient to get a good overall sensitivity in the measurement of the radioactive isotope decay.
- After the β -decay, the daughter nuclei, still confined in the plasma, emit γ -rays, which are detected through an array of HPGe detectors placed around the magnetic trap.
- The in-plasma measured radioactivity is directly correlated to the plasma density and temperature, which will be monitored by a multi-diagnostics setup.

This last correlation represents the crucial point of the experiment allowing mapping the evolution of the half-life of the in-plasma ions with the main plasma parameters and to make a direct comparison with theoretical model predictions.

3.1. Experimental Setup

In the following we will go through a description of the main elements on which the PANDORA experimental setup is based.

Figure 1 shows the overall experimental setup in a render, “at-a-glance”, view. The experimental procedure includes the simultaneous operation of the three main sub-systems: (1) a superconducting magnetic trap allowing plasma generation and confinement; (2) the plasma diagnostics’ system, able to measure the thermodynamic plasma properties (namely, density and temperature); and (3) the array of 14 HPGe detectors for the measurement of the β -decay. Detailed descriptions of each of these three sub-systems will be presented below.

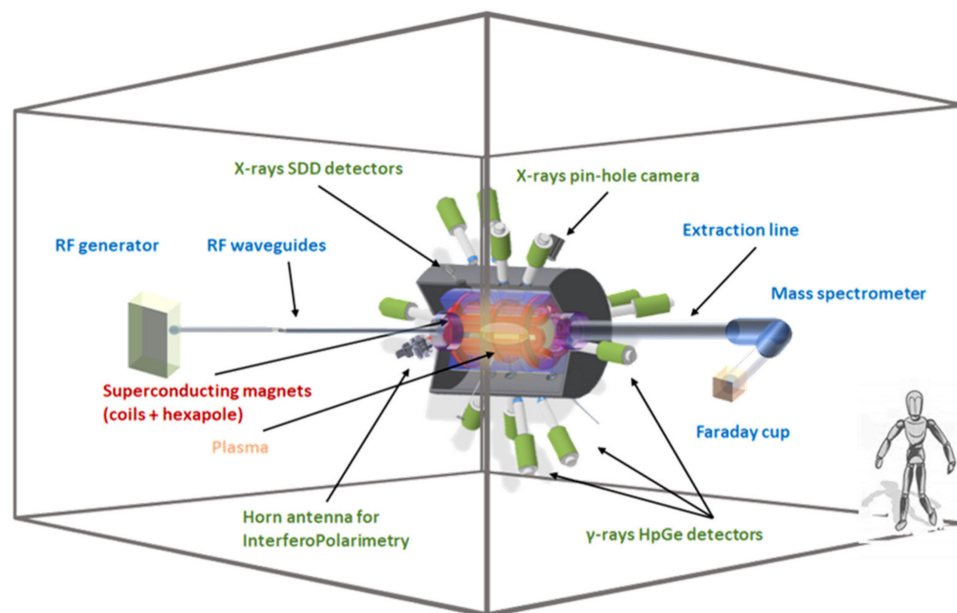


Figure 1. Rendering of the PANDORA setup, including the superconducting magnetic system (in red) inside its cryostat and iron yoke; the array of HPGe detectors; the main diagnostics (optical, X-ray, interfero-polarimetry); the mass spectrometer and the RF system.

3.1.1. Magnetic Trap

The plasma trap uses a strong magnetic field (up to 3 T) for plasma confinement. It consists of a hexapole (i.e., six radial coils) nested inside a group of axial coils (SEXT-IN-SOL configuration). This so-called *minimum-B* configuration produces a superposition of an axial magnetic field (from the axial coils) and a radial magnetic field (from the hexapole coils). Starting from the plasma chamber center, the field grows in every direction, both axially and radially.

The PANDORA magnetic system, shown in Figure 2a, is fully superconductive and consists of:

- # 3 solenoids for axial confinement; and
- # 6 hexapole coils for radial confinement, the hexapole being coaxial with the solenoids.

A single cryostat, surrounded by an iron yoke, will be used for the whole magnetic system (see Figure 2).

The magnetic system has been numerically validated by OPERA and CST microwave studio calculations. The 3D design performed in OPERA is reported in Figure 2a,b. In particular, Figure 2a shows a perspective view of the solenoids and hexapolar coils while Figure 2b includes the cold mass and the lines of sight for radial plasma inspection.

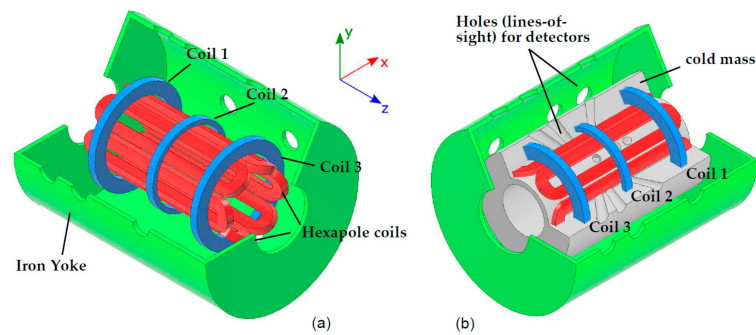


Figure 2. (a) Render 3D view of the magnetic system designed and numerically simulated in OPERA. The plot shows the three axial coils (in blue) plus the hexapolar coils (in red), surrounded by the iron yoke (in green). (b) The same setup of (a), showing also the cold-mass (in gray). The holes (lines of sight) designed to allow radial inspection of the plasma by gamma-ray detectors and plasma diagnostics are included as well.

This set of magnets has specific sizes, reported in Figure 3a, and it will create a minimum-B field configuration, as shown in Figure 3b. The shape of the magnetic field along the z axis and in a plane perpendicular to the Z axis evaluated at $Z = 0$ mm and $R = 140$ mm are shown, respectively, in Figure 3c,d. Due to the specific design, which includes the holes allowing for radial plasma inspection, Figure 3d shows neither a constant azimuthal field (the field varies by 0.1 T over about 1.5 T of average value, corresponding to the gap existing between hexapolar coils) nor a perfect matching with a $\cos(3\theta)$ azimuthal trend, the effect being dependent on the large radius of each hexapolar coil. This was considered a good compromise for the definition of the procurement requirements, with the final executive technical solution being left as part of the tender procedure to build the trap. The magnetic system will surround a cylindrical plasma chamber with inner radius $R_{CH_IN} = 140$ mm and length $L = 700$ mm. The plasma will be heated, starting with 6 kW of RF power at 18 GHz (produced by three klystrons), scalable up to 10 kW and multiple frequency heating in the range of 14–21 GHz.

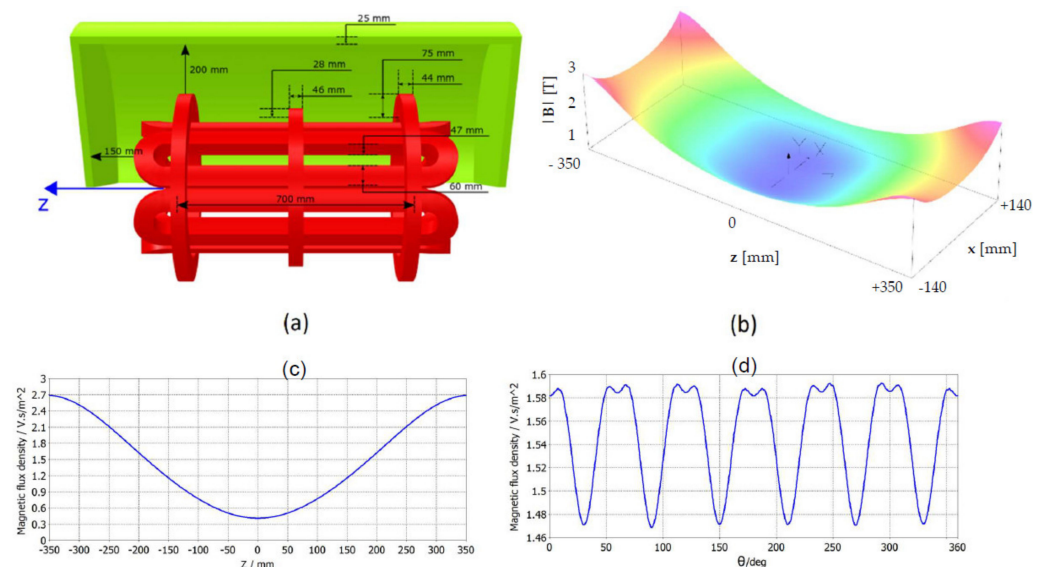


Figure 3. (a) Side view of the PANDORA magnetic system, together with the simulated coil dimensions. Superconducting coils will be contained in a single cryostat surrounded by an iron yoke shown in green. (b) Plot of $|B|$ inside the plasma chamber over the $Y = 0$ plane. (c) Magnetic field module, $|B|$, along the plasma chamber Z axis. (d) Radial field component module, $|B_{hex}|$, of the hexapolar stand-alone structure at $R_{CH_IN} = 140$ mm and $z = 0$ mm, along the azimuthal angle θ .

The magnetic field specifications are summarized in Table 1, where B_{inj} , B_{ext} , B_{min} , and B_{hex} are the magnetic induction module values at the plasma chamber injection ($z = -350$ mm), extraction ($z = 350$ mm), center ($z = 0$ mm), and along its inner wall (radius $R_{CH_IN} = 140$ mm). The magnetic system will be able to operate at any point inside the operative ranges reported in Table 1, but ensuring plasma stability (e.g., fulfilling the rule $B_{min}/B_{ECR} < 0.8$). The trap is requested to operate in liquid-He free mode (i.e., by cryocoolers' modules).

Table 1. PANDORA magnetic field specifications.

Magnetic System Field Specifications	
B_{inj} max @ $z = -350$ mm	3 T
B_{inj} operative range	1.7 T–3 T
B_{ext} max @ $z = 350$ mm	3 T
B_{ext} operative range	1.7 T–3 T
B_{min} @ $z = 0$ mm	0.4 T
B_{hex} @ $R_{CH_IN} = 140$ mm	1.6 T
Liquid He	Free

3.1.2. Isotope Injection System

Gaseous elements are directly injected into the plasma, by connecting gas bottles to a gas injection system. Very precise gas dosing valves allow the injection of the desired amount of the element into the plasma, thus optimizing the consumption. This technique guarantees an efficiency (extracted ions/injected atoms) above 50%, a value leading to a ratio between the ions of the injected gas and the ions of the buffer plasma, which is around 10% or higher.

In the case of solid elements, it is necessary to create a neutral vapor first, or an “ejection” of neutral particles towards the plasma chamber. To this aim, two techniques were mainly used, the resistive oven and the sputtering. In the first case, the ion density amounted to 1–10% of the plasma buffers, depending on the kind of material. In the second case (sputtering), the efficiency dropped to 10% or lower, with a relative concentration around 1%.

In this paper, we briefly describe some key points of the protocol that was elaborated mainly to verify the predicted decrease of the ^{134}Cs lifetime. Such an isotope is commercially available in liquid solutions of HCl: In order to turn it into plasma state, the solution will be dried; the remaining compound will be loaded inside the resistive oven and heated under vacuum inside the trap. At moderate temperatures (<500 °C), the compound sublimates and cesium dissociates, making it available for ionization by plasma electrons. This technique is well established and currently used to produce ^{133}Cs 1+ ion beams in the framework of the SPES project at INFN-LNL [12]. The technique will be further validated by initially carrying out experiments with solutions of ^{133}Cs , using two ECR sources currently installed at INFN-LNS, SERSE, and AISHA, whose magnetic configuration is similar to the one designed for PANDORA. For this purpose, the Standard Temperature Oven (STO) developed at GSI [13] was used. In order to fit the oven into the injection flange of the AISHA ECRIS some mechanical components were modified. Preliminary evaporations test with metallic elements already produced at GSI, such as Zn and Fe, are planned for after the first half of 2022. Since the STO was designed and optimized for the CAPRICE-Type 14.5-GHz ECRIS, several experiments were carried out to investigate the performance of the STO in an 18-GHz ECRIS under different ion source configurations and oven settings.

The results of these feasibility tests are fundamental to plan the next experiments' campaign focused on the evaporation of isotopes such as ^{176}Lu and ^{134}Cs .

3.1.3. HPGe Gamma Ray Detectors' Array

In order to estimate the lifetime of the isotopes, it was necessary to find an efficient detection method to tag the β -decay. Since several physical cases involve the emission

of γ -rays from daughter nuclei with known branching ratios, the total number of decays becomes detectable via γ -rays by means of an array of HPGe detectors. Due to geometrical constraints connected to the realization of the magnetic system, the detector array consisted of 14 HPGe placed around the trap, 12 radially and 2 axially. Detectors could “look” into the plasma through tapered holes made in the cryostat and the external yoke, as shown in Figure 4a. They were placed at a distance of a few centimeters from the yoke in a region of magnetic field whose intensity was about 100 gauss. Figure 4a,b shows details concerning the geometry of the HPGe array around the trap and the shape of the holes made to allow the detection of the gamma-rays. Figure 4c illustrates the results of ray tracing of gammas emitted by the plasma and detected by the array of HPGe detectors, as simulated in GEANT4 [14], while a cut-view of the overall system is displayed in Figure 4d. The total detection efficiency was then determined including the size and shape of plasma and the isotope density inside the trap, assuming detectors with 70% relative efficiency. It ranged between 0.1% and 0.2% depending on the energy of the γ -rays to be detected (see Figure 5).

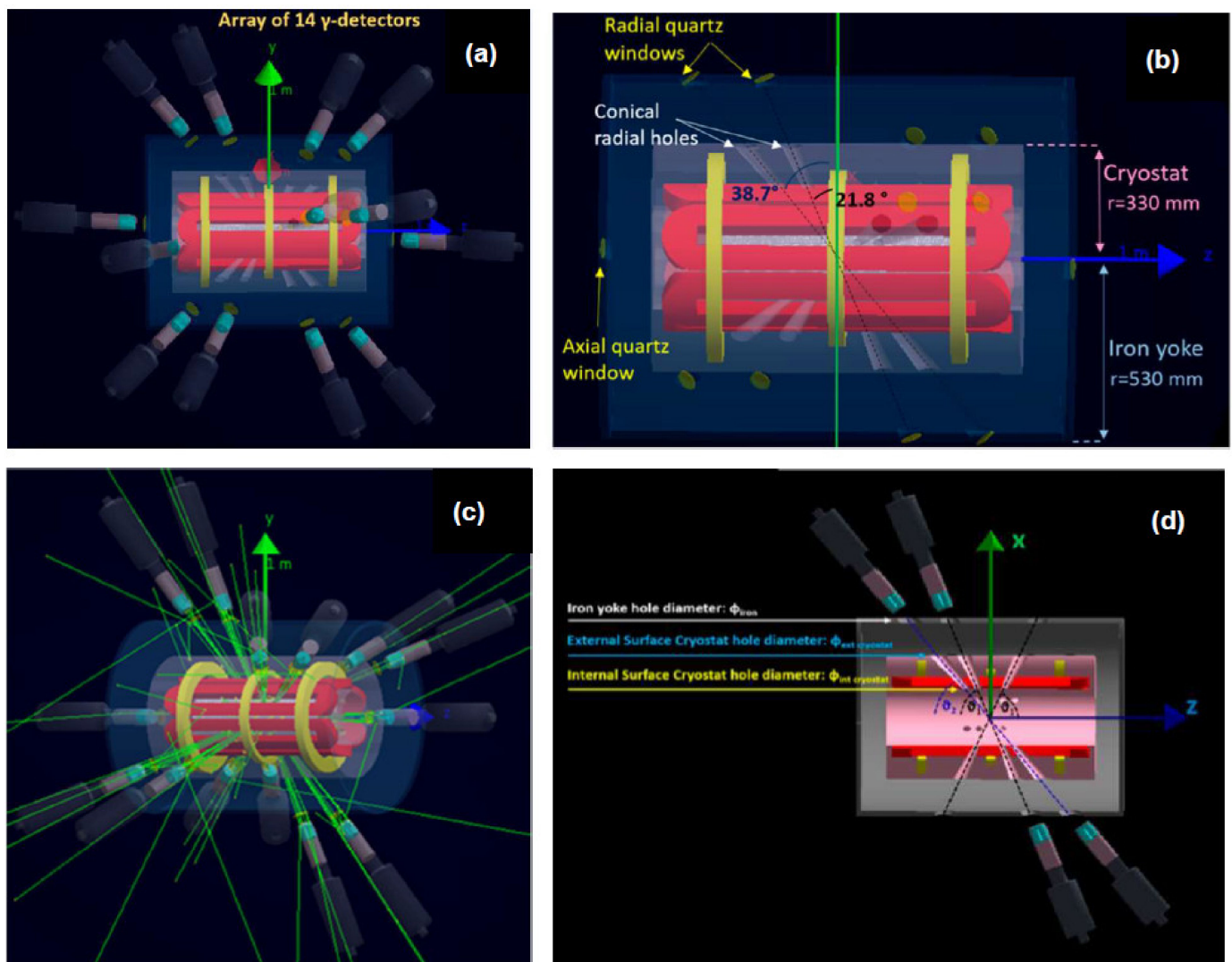


Figure 4. (a–b) Schematic drawings of the trap with holes for HPGe detectors, also including the detectors’ displacement and system sizes. (c) GEANT4 simulations of γ -rays emitted from the plasma considering the magnetic system and detectors array. (d) Cut view of the experimental setup, showing the magnetic system, the lines of sight, and detectors’ positioning.

Although this value seems to be rather low, GEANT4 simulations showed that such an array has the potential to detect the expected variation of the radionuclide half-lives after a measurement time ranging from a couple of weeks for the simplest cases to about 3 months for the longer-living isotopes, as a function of the ionization degree [6,15] (see also Section 4).

The HPGe detectors will work in a rather harsh conditions due to the X-rays' and γ -rays' background of about 50 kHz (in each detector, in terms of detected counts per second) produced inside the plasma trap due to the electron bremsstrahlung. Dedicated electronics able to run in these experimental conditions have been already developed and are currently used by the GAMMA collaboration, which will lend 16 HPGe detectors of the GALILEO Array [16] for the first experimental PANDORA campaign and will share their know-how in the optimization of the setup performances.

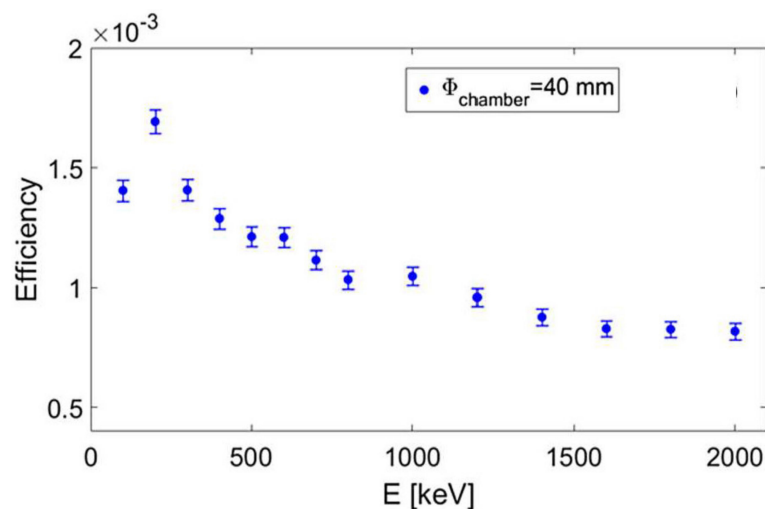


Figure 5. Trend of the detection efficiency of the HPGe array made of 14 detectors having 70% relative efficiency, as a function of the γ -rays' energy.

3.1.4. Multi-Diagnostic System

Diagnostics are crucial to correlate the variation of the decay lifetime to plasma properties. Simultaneous measurements of density and temperature resolved in space and time are thus needed to reconstruct the spatial structure of the plasma and its temporal behavior, in stable and turbulent regimes. In ECR (Electron Cyclotron Resonance) plasmas confined in B_{\min} traps, the energy of the electrons ranges from a few eV to hundreds of keV or even to a few MeV [17] and, since ECRIS plasmas are in non-LTE (non-Local Thermodynamic Equilibrium) conditions, the typical Electron Energy Distribution Function usually consists of three different electron populations: hot, at $kT \sim 100$ keV or more; warm, from $kT \sim 100$ eV up to tens of keV; cold, at $kT \sim 1$ eV \div 100 eV [17].

A complete characterization of ECR plasmas calls for a multiplicity of different tools and analysis methods. To this purpose, our multi-diagnostic setup [18,19] (see Figure 6) will consist of:

- A High-purity Germanium (HPGe) detector for spectral temperature measurement of hard X-rays, including time-resolved spectroscopy.
- A Silicon Drift Detector (SDD) for plasma density and temperature measurements in the warm electron domain.
- Two X-rays pin-hole cameras for 2D space-resolved spectroscopy. Recent developments have also allowed investigating the intensity of the electron losses [20].
- A camera and spectrometer for the plasma-emitted visible light characterization with a resolution of $R = 13,900$ ($\Delta\lambda = 0.035$ nm) at $\lambda = 486$ nm.
- A two-pins' RF probe installed inside the plasma chamber in the injection plate, connected to a Spectrum Analyzer (SA) in order to detect the plasma-emitted EM wave in GHz ranges [21].

- A RF probe connected with a diode and an oscilloscope in order to obtain the time-resolved (but totally integrated) power emitted from the plasma; this value will be used as a trigger signal for instability signature and to perform time-resolved X-ray analysis, via an 80-Gs/s-20-GHz bandwidth oscilloscope.
- A microwave Interferometer and a Microwave Polarimeter for line-integrated total density measurement.

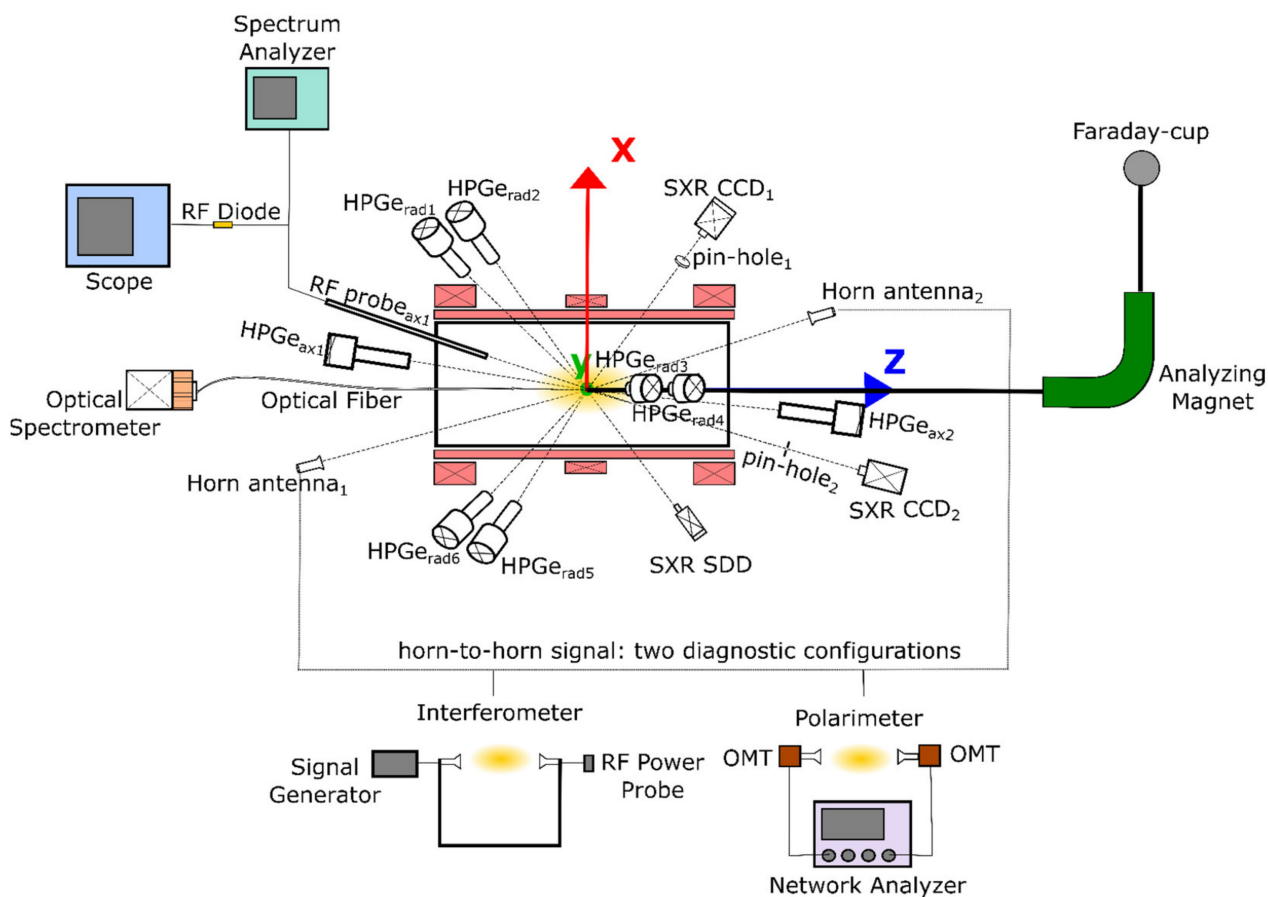


Figure 6. Pictorial sketch of the integrated set of PANDORA diagnostics, highlighting the detectors for X-ray spectroscopy and imaging, optical emission spectroscopy, and microwave imaging and polarimetry.

All diagnostic tools can operate simultaneously with the Faraday cup in order to measure the CSD of ions exiting the setup. The whole set of diagnostics with the related measured plasma parameters, energy, and/or frequency ranges and obtained experimental resolutions/experimental errors is reported in Table 2.

Further upgrades of the multi-diagnostics’ system are ongoing. In particular:

- The spectrograph SARG (*Spettrografo Alta Risoluzione Galileo*) [22] will be able to reach a very high resolution: $R = \lambda/\Delta\lambda = 160.000$, in the range: 370–900 nm, suitable to discriminate plasma-emitted spectra coming from different charge state distributions.
- SARG will operate in addition to the spectrometer by HORIBA© of nominal resolution around 35 picometers ($R = 13,900$ at $\lambda = 486$ nm) that has been already commissioned as a “bridging-the-gap” instrument supporting SARG.
- Concerning X-ray measurements, the INFN-LNS in collaboration with ATOMKI-laboratories (Institute of Nuclear Research, Hungary) recently completed the development of a new Single Photon Counting (SPhC) images’ analysis algorithm, in order to perform pixel-by-pixel energy-resolved investigations [23].
- Microwave Imaging Profilometry (MIP), devoted to an online measurement of local values of the electron density, was successfully experimented on the ECRIS-like

trap ([24,25]). MIP requires the use of probing frequencies much higher than the cyclotron resonance and well above the plasma frequency. Taking into account expected peak values of 10^{12} – 10^{13} cm^{-3} electron density at an ECR frequency of 18 GHz, the so-called V frequency band (50–75 GHz) and W-band (75–110 GHz) can be exploited to reconstruct on-line the plasma shape. This system can be synergic with the polarimeter already planned in the PANDORA multi-diagnostic system.

- An alternative technique for investigating the absolute plasma density, the electron energy distribution functions, and even the electron global drift velocity, is Incoherent Thomson Scattering (ITS). This non-invasive and direct technique, which relies on the scattering of an electromagnetic field on free charges, has a long history of application in the study of diverse high- and low-temperature plasmas. It is now possible to achieve unprecedented sensitivity (measurements in plasma environments with electron densities as low as 10^{10} cm^{-3}). The implementation of a recently developed sensitive diagnostic of this type, known as THETIS [26], will be performed. This technique will be well-suited to the measurement of electron temperatures in the hundreds of eV range, with a potential measurement sensitivity < 1 eV and volumetric resolution on the order of 1 mm^3 . The planned implementation will validate the method as a future diagnostic for PANDORA and also provide key electron property measurements in density and temperature ranges, which will complement the capabilities of other non-invasive diagnostic tools used for electron characterization.

Table 2. List of non-invasive diagnostic tools used in the PANDORA setup, with their most relevant characteristics in terms of sensitivity range, measured plasma parameters, and detection resolution. All these tools have been widely tested in dedicated testbenches, while Thomson Scattering diagnostics’ implementation is ongoing in the PANDORA scenario.

Diagnostic Tool	Sensitive Range	Measurement	Resolution-Measure Error
SDD	1 ÷ 30 keV	Volumetric soft X-ray Spectroscopy: warm electrons’ temperature and density	Resolution~120 eV $\epsilon_{ne} \sim 7\%$, $\epsilon_{Te} \sim 5\%$
HPGe detector	30 ÷ 2000 keV	Volumetric hard X-ray Spectroscopy: hot electrons’ temperature and density	FWHM @ 1332.5 keV < 2.4 keV $\epsilon_{ne} \sim 7\%$, $\epsilon_{Te} \sim 5\%$
Visible Light Camera	1 ÷ 12 eV	Optical Emission Spectroscopy: cold electrons’ temperature and density	$\Delta\lambda = 0.035 \text{ nm}$ $R = 13900$
X-ray pin-hole camera	2 ÷ 15 keV	2D Space-resolved spectroscopy: soft X-ray Imaging and plasma structure	Energy Resolution~0.3 keV Spatial Resolution~0.5 mm
W-band super-heterodyne polarimeter	W-band 90 ÷ 100 GHz	Plasma-induced Faraday rotation: line-integrated electron density	$\epsilon_{ne} \sim 25\%$
Microwave Imaging Profilometry (MIP)	60 ÷ 100 GHz	Electron density profile	$\epsilon_{ne} \sim 1\% \div 13\%$
Multi-pins RF probe	10 ÷ 26.5 GHz	Local EM field intensity	$\epsilon \sim 0.073 \div 0.138 \text{ dB}$
Multi-pins RF probe +	10 ÷ 26.5 GHz	Frequency-domain RF wave	SA Resolution bandwidth: RBW = 3 MHz
Spectrum Analyzer (SA)	(probe range)	Time-resolved radiofrequency burst	80 Gs/s (scope)
Multi-pins RF probe +	10 ÷ 26.5 GHz	and X-ray time-resolved Spectroscopy	time scales below ns
Scope + HPGe detector	(probe range)		
Thomson Scattering	0.5 ÷ 500 eV	EEDF, absolute electron density global electron drift velocity	Condition-dependent (a function of spectral width, dependent on temperature, and area, dependent on density)

4. First Physics’ Cases

The possibility to investigate beta decay rates in stellar-like conditions opens a new scenario in astrophysics and nuclear astrophysics. A major impact on the stellar evolution model can be foreseen if the theoretically predicted lifetime variation will be observed using a plasma trap like the one in PANDORA. The decay is expected to depend on the combination of plasma density and temperature. This combination establishes a given CSD in the plasma in non-LTE (nLTE) conditions, which are the ones occurring in the laboratory plasma. An equivalent CSD can be then extrapolated to LTE scenarios applying to astrophysical plasmas. The most relevant observable is the nuclear decay constant $\lambda(n,T)$, with n and T being the plasma density and temperature, respectively, which shows a very weak dependence on n but a really strong one on T. At a given T, not only the CSD, but also a complex configuration of atomic/electronic excited states in the various ions is achieved in plasma. Hence, ECR plasmas give the unique opportunity to investigate the actual effect of electron temperature on the decay rate, a complementary approach to Storage Rings’

measurements, which investigate the β -decay rate variation due to a single charge state at a time [10]. This provides a more complicated but more coherent and “realistic” picture of the decay, closer to astrophysical contexts than any result based on single-charge evaluation. In the first experimental campaign, we will focus on three cases selected after considering their scientific relevance, the predicted lifetime variation, the natural isotope abundances, and the energy of the gamma-ray emitted by the daughter nuclei populated after the beta decay. The nuclei selected are ^{176}Lu , ^{134}Cs , and ^{94}Nb . The theoretical estimates of their lifetimes, based on the model developed in [27], are reported for each of the selected cases in Figure 7. In particular, the three curves represent ratios of stellar half-life to terrestrial half-life dependence as a function of plasma temperature T^6 , in nLTE conditions. It is evident that at the PANDORA expected electron temperatures their lifetimes are predicted to collapse by several orders of magnitudes, even 6–7 orders of magnitudes around 10 keV in the case of ^{176}Lu .

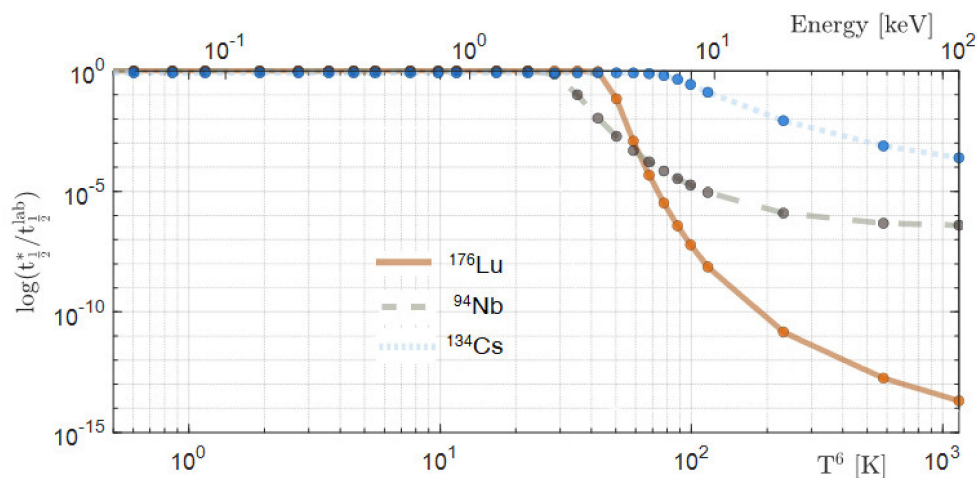


Figure 7. Theoretical estimates (based on [27]) of the ^{176}Lu , ^{134}Cs , and ^{94}Nb ratios of stellar half-life to terrestrial half-life dependence as a function of plasma temperature T^6 [10^6 K] (Energy [keV]) at densities of PANDORA’s plasmas (10^{12} cm^{-3}). The red line corresponds to the trend of ^{176}Lu . The dashed, gray line shows the trend of ^{94}Nb , while the blue, dotted line indicates the trend of ^{134}Cs .

^{176}Lu is a very long-lived nucleus in laboratory conditions and, in principle, might act as a cosmo-chronometer, even if it is known from nuclear physics’ experiments that it is subject to a complex behavior in hot stellar plasmas due to an isomeric state at very low excitation energy, which actually makes it more likely as a thermometer than as a chronometer [28,29]. The s-process branching point at ^{176}Lu is among the most important ones for a precise understanding of slow neutron captures in low and intermediate mass stars. It determines the abundance of ^{176}Hf , which cannot be produced by the r-process because the ^{176}Lu has no viable decay channels in its ground state.

^{134}Cs has a measured half-life of 2 years (as a neutral atom) but predictions suggest that it is reduced to 84 days at a temperature near $kT = 25\text{--}30$ keV [30,31]. Such values roughly mimic the conditions met in the He-shell instabilities (named Thermal pulses) occurring in the final stages of low and intermediate mass stars ($M < 7\text{--}8 M_{\odot}$), approaching for the second time the *Red Giant Branch* and called, for this reason, *Thermally Pulsing Asymptotic Giant Branch* (or TP-AGB) stars [32,33]. Using the present estimates, nucleosynthesis models in stars were not capable to reproduce adequately the observed abundance ratio of the two s-only isotopes, ^{134}Ba and ^{136}Ba . This issue is supposed to have a nuclear origin, and new predictions of the ^{134}Cs half-life, based on more sophisticated nuclear theoretical models, showed a better agreement between models and observations [31]. However, these suggestions call now for an accurate experimental verification, as only a real measurement in a plasma could shed light on the role played by the ionization state on the β -decay half-life.

^{94}Nb nucleus provides the main production channel of ^{94}Mo , in conditions typical of the s process, as this isotope cannot be populated through the r-process (it must, therefore,

derive either from the s-process or from the p-process). The situation met by reaction network calculations in this area is rather peculiar, due to the critical role played by the rather long-lived isotope ^{93}Zr , with a half-life of the same order of magnitude as the typical duration of the TP-AGB phase in low mass stars. Its uniqueness requires a much better knowledge of the ^{94}Nb β -decay lifetime, achievable only through a direct measurement in stellar conditions.

According to the estimated lifetimes in plasma, since the harsh environment (the noise is represented by the intense plasma self-emission) strongly affects the signal-to-noise ratio, simulations of a real experimental run were performed to estimate the run duration to get statistically meaningful results, in terms of σ -levels of significance. Figure 8 reports one of these simulations for the case of ^{176}Lu . The first (from the left) green vertical axis reports a decreasing lifetime expressed in years, starting from the lifetime of the neutral isotope. Assuming a plasma of 1500 cm^3 in volume with a concentration of 1% of Lu with respect to the buffer density (10^{13} ions/cm^3), it was possible to estimate, at a given value of lifetime, the effective in-plasma Lu activity. This is shown in the second, blue vertical axis. Finally, including the efficiency of the HPGe detector array estimated by the above mentioned GEANT4 simulations, we evaluated the counting rate of the detector array shown in the third, black vertical axis. The x-axis reports the measurement time. Pseudo-colors give the total number of counts at the peak of interest (i.e., the Hf-emitted gamma-rays, around 307 keV). To estimate the plasma self-emitted X-ray background, it was considered the emission of a plasma at 10 keV of temperature (starting from a measured scenario at smaller plasma sizes and densities than PANDORA, but rescaling the numbers), and the error over this background was taken as the square root of counts in the energy resolution window, while the counts due to the real decays occurring in the plasma were summed up linearly with time.

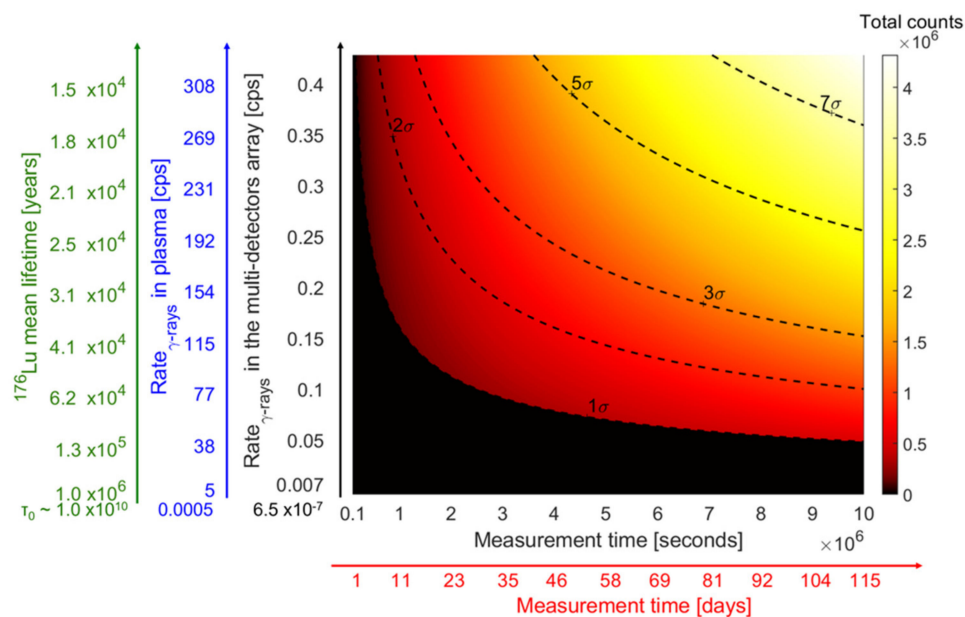


Figure 8. Measurability plot reporting the confidence levels that it is possible to obtain vs. the decay rate (or the lifetime) of the ^{176}Lu and the measurement time.

The dashed lines indicate the n-sigma confidence levels at each combination of detected rate and measurement time. Depending on the relevance of lifetime decrease, the measurements are deemed to last from a few days (in the case of 6 orders of magnitude collapse) up to 3 months. Similar plots can be obtained for ^{134}Cs and ^{94}Nb . Due to their shorter lifetime even in the neutral case, the needed quantities for these two nuclides are much smaller than for the ^{176}Lu : e.g., a density of 10^6 cm^{-3} of ^{134}Cs ions should be sufficient to get 3-sigma levels of significance already after 10–15 h, at the expected in-plasma lifetime.

Study of Plasma Opacity for Compact Binary Objects

Plasma opacity has a great impact on energy transport and spectroscopic observations in many astrophysical objects. Particularly relevant is the role played by the opacity during electromagnetic *transients* emitted from compact binary mergers (*kilonovae* (KN)), as it delivers information on the post-merging plasma ejecta composition (relying on r-process nucleosynthesis yields) [34]. A large uncertainty factor, greatly complicating theoretical interpretations, arises from an almost total ignorance on ejecta opacity data at the typical conditions of a KN event. Trapped magneto-plasmas conceived in PANDORA may open the route to experimental in-laboratory measurements of opacities at electron densities and temperatures resembling some ejecta plasma conditions, contributing, therefore, to shed light on r-process-generated metallic species at specific time stages of KN diffusion [35]. In Figure 9a numerical results about expected opacities for the most relevant physics cases are presented, as a function of plasma T_e . Figure 9b reports about mean opacities for some relevant r-process elements as expected at different electron fractions Y_e .

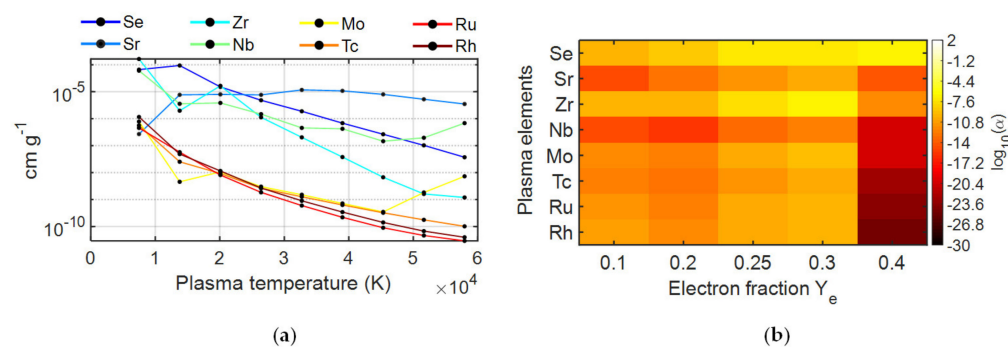


Figure 9. (a) Mean opacity (in $\text{cm} \cdot \text{g}^{-1}$) vs. plasma temperature (at $n_0 = 10^{12} \text{ cm}^{-3}$) assuming a plasma emission spectrum arising from numerical radiative transfer equation simulations. (b) Weighted mean opacity (α) for r-process element abundances (elements vs. neutron richness) at $kT = 0.65 \text{ eV}$ and n_0 . The weighting was performed by using relative abundances of species resulting from SKYNET [36] nuclear network calculations of r-process nucleosynthesis yields as a function of Y_e .

5. Conclusions

A new experimental setup to study the β -decay rate of radioisotopes of astrophysical interest in an ionized plasma is under development. Here, we presented an overview of the setup built around a compact plasma trap, its main features, the gamma detection array used, the experimental method proposed, and its expected impact in nuclear astrophysics. The PANDORA setup is expected to come into operation in 2024, with the first experimental campaign focused on the study of three physics cases, ^{176}Lu , ^{134}Cs , and ^{94}Nb . An important breakthrough in stellar evolution and nucleosynthesis models is foreseen if the predicted lifetime variations are observed.

Author Contributions: Conceptualization, D.M., D.S., M.B., L.C. (Luigi Cosentino), S.C., C.D.A., G.D.A., J.-E.D., A.G., S.G., R.K., M.L.C., S.L., A.M. (Alberto Mengoni), B.M., E.N., F.O., A.P. (Angelo Pidotella), S.T. (Simone Taioli), G.T. and S.T. (Sedina Tsikata); Data curation, D.M., S.A., V.A., V.P.B., S.B., D.D.S., L.D.D., U.F., G.S.M., M.M. (Maria Mazzaglia), E.N., A.P. (Albino Perego), R.R. (Richard Rácz), A.D.R., F.R., S.S. (Stefano Simonucci), G.S. (Gino Sorbello), R.S., S.T. (Simone Taioli), G.T., S.T. (Sedina Tsikata) and D.V.; Formal analysis, V.A., A.B., M.B., S.C., K.-L.K., A.L., G.M., A.M. (Alberto Mengoni), B.M., A.P. (Albino Perego), A.P. (Angelo Pidotella), M.R., S.S. (Stefano Simonucci), S.T. (Simone Taioli), G.T. and D.V.; Funding acquisition, D.M., D.S., Investigation, S.B. (Sándor Biri), A.G., F.O., A.P. (Albino Perego), R.R. (Richard Rácz), S.S. (Stefano Simonucci) and G.T.; Methodology, D.S., S.B. (Sándor Biri), S.B., M.B., L.C. (Luigi Celona), G.D.A., L.D.D., A.E.V., U.F., A.G., C.S.G., S.L., M.M. (Mario Maggiore), F.M., L.M. (Laurent Maunoury), G.S.M., M.M. (Maria Mazzaglia), D.R.N., E.N., L.P., G.P., S.P. (Santi Pavone), S.P. (Salvatore Pennisi), R.R. (Richard Rácz), R.R. (Riccardo Reitano), G.S. (Gaetano Schillaci), S.S., G.S. (Gino Sorbello), K.T. and A.T. (Antonio Trifirò); Project administration, V.P.B., A.M. (Andrea Miraglia), M.M. (Mario Musumeci) and G.S. (Gaetano Schillaci); Resources, L.C. (Luigi Celona), M.C., T.I., R.K., M.L.C., F.M., L.M. (Luciana Malferrari),

D.R.N., F.O., G.P., A.P. (Angelo Pidotella), R.R. (Riccardo Reitano), D.R. and K.T.; Software, S.A., L.A., J.-E.D., L.D.D., C.S.G., G.S.M., B.M., E.N., A.P. (Angelo Pidotella) and F.R.; Supervision, D.M., M.B., S.G., A.M. (Alberto Mengoni) and G.T.; Validation, D.M., K.-L.K., M.M. (Mario Maggiore), D.R., R.S. and A.T. (Aurora Tumino); Visualization, M.C., H.K., M.M. (Mario Musumeci), D.R., A.T. (Antonio Trifirò) and L.V.; Writing—original draft, D.M., D.S., M.B., F.M., L.M. (Laurent Maunoury), G.S.M., A.M. (Alberto Mengoni), E.N., A.P. (Angelo Pidotella), G.T. and S.T. (Sedina Tsikata); Writing—review & editing, S.B. (Sándor Biri), A.B., V.P.B., L.C. (Luigi Celona), L.C. (Luigi Cosentino), S.C., M.C., C.D.A., G.D.A., J.-E.D., D.D.S., A.G., T.I., H.K., M.L.C., D.R.N., F.O., R.R. (Richard Rácz), F.R., S.S. (Stefano Simonucci), S.T. (Simone Taioli), A.T. (Aurora Tumino) and L.V. All authors have read and agreed to the published version of the manuscript.

Funding: The authors gratefully acknowledge the 3rd Nat. Committee of INFN support and funding of the PANDORA_Gr3 project.

Institutional Review Board Statement: Not applicable.

Informed Consent Statement: Not applicable.

Data Availability Statement: Data are available upon request.

Acknowledgments: The contribution and activity of Simone Taioli was partially funded by the Ministry of Science and Higher Education of the Russian Federation (World Class Research Center program: Advanced Digital Technologies, contract No. 075-15-2020-934; 17 November 2020).

Conflicts of Interest: The authors declare no conflict of interest.

References

1. Emery, G.T. Perturbation of nuclear decay rates. *Ann. Rev. Nucl. Sci.* **1972**, *22*, 165–202. [[CrossRef](#)]
2. Simonucci, S.; Taioli, S.; Palmerini, S.; Busso, M. Theoretical estimates of Stellar e-Captures. I. The half-life of ^7Be in evolved stars. *Astrophys. J.* **2013**, *764*, 118. [[CrossRef](#)]
3. Bahcall, J.N. Theory of Bound-State Beta Decay. *Phys. Rev.* **1961**, *124*, 495. [[CrossRef](#)]
4. Bosch, F.; Faestermann, T.; Friese, J.; Heine, F.; Kienle, P.; Wefers, E.; Zeitelhack, K.; Beckert, K.; Franzke, B.; Klepper, O.; et al. Observation of bound state β decay of fully ionized ^{187}Re : ^{187}Re – ^{187}Os cosmochronometry. *Phys. Rev. Lett.* **1996**, *77*, 5190. [[CrossRef](#)] [[PubMed](#)]
5. Jung, M.; Bosch, F.; Beckert, K.; Eickhoff, H.; Folger, H.; Franzke, B.; Gruber, A.; Kienle, P.; Klepper, O.; Koenig, W.; et al. First observation of bound state β decay. *Phys. Rev. Lett.* **1992**, *69*, 2164. [[CrossRef](#)]
6. Mascali, D.; Busso, M.; Mengoni, A.; Amaducci, S.; Guiseppe, C.; Celona, L.; Cosentino, G.; Cristallo, S.; Finocchiaro, P.; Galata, A.; et al. The PANDORA project: An experimental setup for measuring in-plasma β -decays of astrophysical interest. *EPJ Web Conf.* **2020**, *227*, 01013. [[CrossRef](#)]
7. Mascali, D.; Musumarra, A.; Leone, F.; Romano, F.P.; Galata, A.; Gammino, S.; Massimi, C. PANDORA, a new facility for interdisciplinary in-plasma physics. *Eur. Phys. J. A* **2017**, *53*, 145. [[CrossRef](#)]
8. Metzger, B. FRIB Summer School Lecture on “Kilonovae”. 2018. Available online: https://indico.fnal.gov/event/15789/attachments/20936/26096/Metzger_FRIB_kilonovae.pdf (accessed on 14 May 2018).
9. Burbidge, M.E.; Burbidge, G.R.; Fowler, W.A.; Hoyle, F. Synthesis of the elements in stars. *Rev. Mod. Phys.* **1957**, *29*, 547. [[CrossRef](#)]
10. Litvinov, Y.; Bosch, F. Beta decay of highly charged ions. *Rep. Progr. Phys.* **2011**, *74*, 016301. [[CrossRef](#)]
11. Tanaka, M.; Kato, D.; Gaigalas, G.; Kawaguchi, K. Systematic opacity calculations for Kilonovae. *Mon. Not. R. Astron. Soc.* **2020**, *496*, 1369. [[CrossRef](#)]
12. Galatà, A.; Roncolato, C.; Bisoffi, G.; Francescon, P.; Bellan, L.; Bermudez, J.; Bortolato, D.; Comunian, M.; Conte, A.; De Lazzari, M.; et al. Towards the first beams from the ADIGE injector for the SPES Project. *J. Phys. Conf. Ser.* **2019**, *1350*, 01209. [[CrossRef](#)]
13. Tinschert, K.; Lang, R.; Mäder, J.; Maimone, F.; Roßbach, J. Metal ion beam production with improved evaporation ovens. In Proceedings of the 20th International Workshop on Electron Cyclotron Resonance Ion Sources (ECRIS-2012), JaCoW-WEPP15, Sydney, Australia, 25–28 September 2012.
14. Agostinelli, S.; Allison, J.; Amako, K.A.; Apostolakis, J.; Araujo, H.; Arce, P.; Asai, M.; Axen, D.; Banerjee, S.; Barrand, G.J.N.I.; et al. GEANT4—A Simulation Toolkit. *Nucl. Inst. Meth. A* **2003**, *506*, 250–303. [[CrossRef](#)]
15. Naselli, E.; Mascali, D.; Caliri, C.; Castro, G.; Celona, L.; Galata, A.; Gammino, S.; Mazzaglia, M.; Romano, F.P.; Guiseppe, T.; et al. Nuclear β -decays in plasmas: How to correlate plasma density and temperature to the activity. *EPJ Web Conf.* **2020**, *227*, 02006. [[CrossRef](#)]
16. Goasduff, A.; Mengoni, D.; Recchia, F.; Valiente-Dobon, J.J.; Menegazzo, R.; Benzoni, G.; Barrientos, D.; Bellato, M.; Bez, N.; Biasotto, M.; et al. The GALILEO g-ray array at the Legnaro National Laboratories. *Nucl. Instrum. Methods Phys. Res. Sect. A Accel. Spectrometers Detect. Assoc. Equip.* **2021**, *1015*, 165753. [[CrossRef](#)]
17. Geller, R. *Electron Cyclotron Resonance Ion Sources and ECR Plasmas*; PA Institute of Physics: Philadelphia, PA, USA, 1996.

18. Naselli, E.; Mascali, D.; Biri, S.; Caliri, C.; Castro, G.; Celona, L.; Consetino, L.G.; Galata, A.; Gammino, S.; Giarrusso, M.; et al. Multidiagnostics setups for magnetoplasmas devoted to astrophysics and nuclear astrophysics research in compact traps. *J. Instrum.* **2019**, *14*, C10008. [[CrossRef](#)]
19. Biri, S.; Palinkas, J.; Perduk, Z.; Racz, R.; Caliri, C.; Castro, G.; Celona, L.; Gammino, S.; Mazzaglia, M.; Naselli, E.; et al. Multi diagnostic setup at the Atomki-ECRIS to investigate the two-close-frequency heating phenomena. *J. Instrum.* **2018**, *13*, C11016. [[CrossRef](#)]
20. Naselli, E.; Racz, R.; Biri, S.; Mazzaglia, M.; Galata, A.; Celona, L.; Gammino, S.; Torrisci, G.; Mascali, D. Quantitative analysis of an ECR Ar plasma structure by X-ray spectroscopy at high spatial resolution. *J. Instrum.* **2022**, *17*, C01009.
21. Torrisci, G.; Mascali, D.; Sorbello, G.; Castro, G.; Celona, L.; Gammino, S. Numerical and experimental characterization of RF waves propagation in ion sources magnetoplasmas. *IEEE Trans. Antennas Propagat.* **2019**, *67*, 2142. [[CrossRef](#)]
22. Giarrusso, M.; Avila, G.; Del Zanna, G.; Landi, E.; Leone, F.; Munari, M.; Castro, G.; Celona, L.; Gammino, S.; Mascali, D.; et al. High resolution spectropolarimetry: From Astrophysics to ECR plasmas. *J. Instrum.* **2018**, *13*, C11020. [[CrossRef](#)]
23. Naselli, E.; Racz, R.; Biri, S.; Mazzaglia, M.; Celona, L.; Gammino, S.; Torrisci, G.; Perduk, Z.; Galata, A.; Mascali, D. Innovative Analytical Method for X-Ray Imaging and Space-Resolved Spectroscopy of ECR Plasmas. *Condens. Matter* **2022**, *7*, 5. [[CrossRef](#)]
24. Di Donato, L.; Morabito, A.F.; Torrisci, G.; Isernia, T.; Sorbello, G. Electromagnetic Inverse Profiling for Plasma Diagnostics via Sparse Recovery Approaches. *IEEE Trans. Plasma Sci.* **2019**, *47*, 1781–1787. [[CrossRef](#)]
25. Di Donato, L.; Mascali, D.; Morabito, A.F.; Sorbello, G. A Finite-Difference Approach for Plasma Microwave Imaging Profilometry. *J. Imaging* **2019**, *5*, 70. [[CrossRef](#)] [[PubMed](#)]
26. Vincent, B.; Tsikata, S.; Mazouffre, S.; Minea, T.; Fils, J. A compact new incoherent Thomson scattering diagnostic for low-temperature plasma studies. *Plasma Sources Sci. Technol.* **2018**, *27*, 055002. [[CrossRef](#)]
27. Takahashi, K.; Yokoi, K. Beta-Decay Rates of Highly Ionized Heavy Atoms in Stellar Interiors. *At. Data Nucl. Data Tables* **1983**, *36*, 375. [[CrossRef](#)]
28. Klay, N.; Käppeler, F.; Beer, H.; Schatz, G.; Börner, H.; Hoyler, F.; Robinson, S.J.; Schreckenbach, K.; Krusche, B.; Mayerhofer, U.; et al. Nuclear structure of ^{176}Lu and its astrophysical consequences. I. Level scheme of ^{176}Lu . *Phys. Rev. C* **1991**, *44*, 2801. [[CrossRef](#)] [[PubMed](#)]
29. Klay, N.; Käppeler, F.; Beer, H.; Schatz, G. Nuclear structure of ^{176}Lu and its astrophysical consequences II. ^{176}Lu , a thermometer for stellar helium burning. *Phys. Rev. C* **1991**, *44*, 2839. [[CrossRef](#)]
30. Palmerini, S.; Busso, M.; Vescovi, D.; Naselli, E.; Pidotella, A.; Mucciola, R.; Cristallo, S.; Mascali, D.; Mengoni, A.; Simonucci, S.; et al. Presolar Grain Isotopic Ratios as Constraints to Nuclear and Stellar Parameters of Asymptotic Giant Branch Star Nucleosynthesis. *Astrophys. J.* **2021**, *921*, 7. [[CrossRef](#)]
31. Taioli, S.; Vescovi, D.; Busso, M.; Palmerini, S.; Cristallo, S.; Mengoni, A.; Simonucci, S. Theoretical estimate of the half-life for the radioactive ^{134}Cs and ^{135}Cs in astrophysical scenarios. *arXiv* **2021**, arXiv:2109.14230.
32. Cristallo, S.; Straniero, O.; Gallino, R.; Piersanti, L.; Dominguez, I.; Lederer, M.T. Evolution, Nucleosynthesis, and Yields of Low-mass Asymptotic Giant Branch Stars at Different Metallicities. II. The FRUITY Database. *Astrophys. J. Suppl.* **2011**, *197*, 17. [[CrossRef](#)]
33. Busso, M.; Gallino, R.; Wasserburg, G.J. Nucleosynthesis in Asymptotic Giant Branch Stars: Relevance for Galactic Enrichment and Solar System Formation. *Ann. Rev. Astron. Astrophys.* **1999**, *37*, 239. [[CrossRef](#)]
34. Burns, E. Neutron star mergers and how to study them. *Living Rev. Relativ.* **2020**, *23*, 1–177. [[CrossRef](#)]
35. Pidotella, A.; Cristallo, S.; Galata, A.; La Cognata, M.; Mazzaglia, M.; Perego, A.; Tumino, A.; Vescovi, D.; Mascali, D. In Plasma study of opacity relevant for compact binary ejecta. *Nuovo Cim. C* **2021**, *44*, 65.
36. Lippuner, J.; Roberts, L.F. SkyNet: A Modular Nuclear Reaction Network Library. *Astrophys. J. Suppl.* **2017**, *233*, 18. [[CrossRef](#)]